Journal of Power Sources 196 (2011) 3736–3742

Contents lists available at ScienceDirect

Journal of Power Sources

journal homepage: www.elsevier.com/locate/jpowsour

Application of complementary analytical tools to support interpretation of polymer-electrolyte-membrane fuel cell impedance data

Sunil K. Roy, Helena Hagelin-Weaver, Mark E. Orazem*

Department of Chemical Engineering, University of Florida, Gainesville, FL 32611, United States

ARTICLE INFO

Article history:
Received 2 November 2010
Received in revised form
14 December 2010
Accepted 14 December 2010
Available online 24 December 2010

Keywords:
X-ray diffraction
X-ray photoelectron spectroscopy
Transmission electron microscopy
Scanning electron microscopy
Capacitance
Impedance spectroscopy

ABSTRACT

A series of ex situ techniques, including scanning electron microscopy, transmission electron microscopy, X-ray photoelectron spectroscopy, X-ray diffraction, and inductively coupled plasma-mass spectroscopy were used to study morphological and chemical changes associated with the aging of a membrane electrode assembly in a polymer-electrolyte-membrane fuel cell. These results were correlated with the results of in situ electrochemical measurements, including measurement of steady-state polarization curves and electrochemical impedance spectroscopy. The results support the premise that the low-frequency inductive features seen in the impedance response provide information useful for understanding phenomena, such as platinum oxidation, that lead to reduction of fuel cell performance. The reduction in electrochemically active surface area, obtained from the high-frequency part of the impedance response, was consistent with the observed agglomeration of platinum particles and platinum oxidation.

1. Introduction

Low-frequency inductive features [1–3] are commonly seen in impedance spectra for polymer-electrolyte-membrane (PEM) fuel cells (see, for example, Fig. 3 reported by Makharia et al. [1]). Roy and Orazem [4] used the measurement model approach developed by Agarwal et al. [5–8] to demonstrate that, for the fuel cell under steady-state operation, the low-frequency inductive loops were consistent with the Kramers–Kronig relations. Thus, the low-frequency inductive loops could be attributed to process characteristics rather than to non-stationary artifacts.

Roy et al. [9] showed that both a reaction mechanism invoking formation of an adsorbed peroxide intermediate and a mechanism involving formation of a platinum oxide could give rise to the inductive loops. The role of peroxide intermediates in the oxygen reduction reaction is supported by independent observation of hydrogen peroxide formation in PEM fuel cells [10–12]. The mechanism involving formation of a platinum oxide was motivated by the work of Darling and Meyers [13], who showed that a model invoking platinum oxidation and subsequent dissolution provided good agreement with experimental observations. Platinum dissolution has been observed in PEM fuel cells which can lead to the loss of catalytic activity and, consequently, to the degradation of the fuel cell performance [14]. Mathias et al. [15] developed a model for the influence of platinum oxidation on impedance response in which the oxide was assumed to be comprised primarily of PtOH. Their model associated the inductive loop seen at low frequency with platinum oxidation.

A number of workers have explored the physical and chemical changes associated with aging. Roth et al. [16] showed that, for carbon-supported Pt–Ru–WO_x catalysts, surface-sensitive XPS measurements detected metallic platinum, platinum oxide and hydroxide species, metallic Ru, ruthenium oxide, hydrous ruthenium oxide and WO_3. Xie et al. [17,18] reported, using TEM, SEM, and electrocatalytic surface area measurement, that agglomeration of catalyst particles, migration of metal catalyst particles, and degradation of the recast Nafion® ionomer network occurred during operation under high humidity conditions. Ferreira et al. [19] showed that the formation of soluble platinum species, such as Pt^{2+}, plays an important role in platinum surface loss in PEMFC electrodes. Chatenet et al. [20] report that chemical (EDS and XPS) and physical (SEM and TEM) techniques revealed dissolution and redistribution of catalyst within the MEA. Zhang et al. [21] report XPS and scanning electron microscopy results that show that the ionomer on the catalyst layer degraded or decreased in concentration after fuel cell operation.

A recent review by Zhang et al. [22] illustrates major degradation processes and emphasizes PtO_x formation and degradation. Zhang et al. [23] employed XPS to investigate degradation pro-

* Corresponding author at: Department of Chemical Engineering, University of Florida, PO Box 116005, Gainesville, FL 32611, United States. Tel.: +1 352 392 6207; fax: +1 352 392 9513.
E-mail address: meo@che.ufl.edu (M.E. Orazem).

0378-7753/$ – see front matter © 2010 Elsevier B.V. All rights reserved.
doi:10.1016/j.jpowsour.2010.12.069

cesses, including carbon and Pt dissolution, in a PEM fuel cell. Rinaldo et al. [24] provided a physical model for Pt–O formation and Pt dissolution that was validated by experimental data. Liu et al. [25] verified formation of platinum oxide and reported it to be a reversible process. Their observed surface coverage was in good agreement with the model proposed by Darling and Meyers [13]. Zhang et al. [26] reported PtO_x formation under open-circuit operation. Impedance spectroscopy data were reported, but were fit to an equivalent electrical circuit.

The impedance data presented by Roy et al. [9] was interpreted in terms of a model that accounted for mass transfer and proposed kinetic mechanisms, including reversible formation and dissolution of PtO_x following Darling and Meyers [13]. As discussed by Orazem and Tribollet [27], even mechanistic models for impedance spectroscopy are not unique and must be supported by independent observations. The object of this work was to perform experiments which may provide evidence of the reaction mechanisms proposed in previous work [9]. The unique feature of the present work is that the ex situ analysis is coupled with interpretation of impedance features in terms of catalyst oxidation reactions.

2. Experimental

The techniques used included electrochemical impedance spectroscopy, scanning electron microscopy (SEM), transmission electron microscopy (TEM), X-ray photoelectron spectroscopy (XPS), X-ray diffraction (XRD), and inductively coupled plasma-mass spectroscopy (ICP-MS). The experimental system and the impedance instrumentation used are presented in this section.

2.1. Materials and chemicals

The membrane electrode assembly (MEA) (purchased from Ion Power, Inc., New Castle, DE) employed 0.0508 mm (2 mil) thick Nafion® N112 with catalyst layers of about 0.025 mm thickness on both sides of the membrane. The active superficial surface area was 5 cm^2. The catalyst layers were platinum supported on carbon with a Pt catalyst loading of 0.4 mg cm^{-2} on both the anode and the cathode sides. The gas diffusion layer (GDL) used had an effective thickness of 0.284 mm, and was made of carbon cloth with uniform macro-pores. The flow channel used was of serpentine configuration. The material of the flow channel was graphite with the outlet lower than the inlet to facilitate removal of condensed water. A torque of 45 in. pounds was applied to the fuel cell assembly. Hydrogen gas was used as fuel and a 79% N_2 and 21% O_2 mixture was used as oxidant. Compressed N_2 was used to purge the fuel cell before and after experiments. A Barnstead E-Pure Water System with an ion resistivity of 14.9 MΩ cm was used as a source of deionized water delivered to the anode and the cathode humidifiers.

An 850C fuel-cell test station (supplied by Scribner Associates, Southern Pines, NC) was used to control reactant flow rates and temperatures. The test station was connected to a computer by an interface for data acquisition. The gas flows were humidified to 100% relative humidity at the respective temperatures. The hydrogen flow rate was 0.1 l min^{-1}, and the air flow rate was 0.5 l min^{-1}. The maximum stoichiometry for hydrogen and air was 1.5 and 2.5, respectively, and the cell was operated at the fully humidified condition.

2.2. Electrochemical impedance spectroscopy

Impedance measurements were performed with the 850C fuel-cell test station, which contains an electronic load and impedance measurement capability. All electrochemical measurements were performed with a two-electrode cell. The anode was used as a pseudo-reference electrode. The impedance measurements were conducted in galvanostatic mode for a frequency range of 10 kHz to 5 mHz with a 10 mA peak-to-peak sinusoidal perturbation. The corresponding potential perturbation ranged from 0.04 mV to 0.4 mV. Following the recommendations of Hirschorn et al. [28], the perturbation amplitude selected was the largest amplitude that did not cause visible distortions in low-frequency Lissajous plots. The frequencies were spaced in logarithmic progression with 10 points per frequency decade. Impedance scans were conducted in auto-integration mode with a minimum of 2 cycles per frequency measured.

2.3. Aging protocol for the samples

The un-used sample was analyzed as received from the vendor. The aged sample was used in the fuel cell for a period of 3 months with frequent start-stop cycles and operation at various steady current loads for approximately 9 h per day and a total period of 600 h.

2.4. Surface analysis

Several analysis techniques were employed to study the morphology, sintering, and oxidation state of elements in the cathode catalyst layer of the MEA.

2.4.1. Scanning electron microscopy

SEM images were collected from un-used and used samples with a JOEL JSM 6400. For sample preparation, a small portion from the center of the both un-used and used MEA was cut with sharp razor.

2.4.2. Transmission electron microscopy

The TEM analysis was performed with a JOEL JSM-2010F Field Emission Electron Microscope, equipped with an energy dispersive spectrometer (EDS) for compositional analysis. The TEM micrographs were collected at 200 kV accelerating voltage for several magnifications in bright field mode (transmitted electrons). The samples were prepared following a procedure reported in the literature [29]. A small portion from the center of both the un-used and used MEAs were cut with sharp razor and embedded in epoxy resin (Araldite 5002) for 48 h at 60 °C. Thin (90 nm) sections from the membrane-electrodes interfaces were then cut with a diamond knife on Reichert OMU3 ultramicrotome at room temperature. The samples were mounted on Cu grids (mesh size 200) prior to TEM study.

2.4.3. X-ray photoelectron spectroscopy

The XPS scans were collected with a PHI 5100 ESCA system by Perkin-Elmer. The X-ray source was a Mg anode with a work function of 4.8 eV. The emitted electrons were collected at a 45° angle with respect to the sample. The sample was scanned at 300 W power in the binding-energy range from 1000 to 0 eV with a step of 0.5 eV and 30 ms per step. The full-scan survey was generated at a pass energy of 89.45 eV; whereas, the narrow scans (high resolution) for several peaks were performed at a pass energy of 22.36 eV. The XPS data were used to analyze the surface (10–15 atomic layers) of the MEA cathode catalyst layers before and after use. The analysis was facilitated by the fact that the gas-diffusion layer had not been hot-pressed onto the membrane electrode assembly before use in the fuel cell. A small portion from the center of both un-used and used MEA cathode catalyst layer were cut with sharp razor and mounted on a sample holder. Elements present on the surface were identified according to binding energies from reference elements and compounds. The high-resolution spectra were processed using an 11-point, 2nd-order, Savitsky-Golay smoothing routine, followed by a Shirley background subtraction to obtain a

zero baseline. All the XPS spectra presented were normalized to the highest intensity peak.

2.4.4. X-ray diffraction

The XRD data were gathered on a Philips powder X-ray diffractometer using Bragg–Brentano geometry with Cu-Kα radiation (λ = 1.54 Å). Diffraction patterns were obtained for both the un-used and the used cathode catalyst layers, which were secured onto a glass side with double-sided sticky tape. Average platinum particle sizes were calculated from the line-broadening of the XRD peaks using the Scherrer equation

$$\tau = \frac{K\lambda}{\beta \cos\theta} \quad (1)$$

where K is the dimensionless shape factor, generally taken as unity, λ is the wavelength of the incident radiation, β is the line broadening at half the maximum intensity (full width at half maximum (FWHM)), and θ is the peak position.

3. Results

The electrochemical responses of the un-used and used MEAs were measured to determine any difference in performance due to extended use. The catalyst layers and MEAs were also characterized using several analytical techniques in an attempt to determine the properties leading to the variation in the electrochemical response. The results from the effluent analysis are also presented.

3.1. Electrochemical response

The performances of the fuel cell with a un-used MEA, as well as with an MEA after 600 h of operation were investigated using measurement of polarization curves and impedance spectra. As presented in Fig. 1, a sharp decrease in the current density was observed after extended operation. This is particularly apparent in the ohmic and mass-transport-limited regimes of the polarization curve.

The corresponding impedance response, presented in Fig. 2, shows that the impedance increased significantly for the aged MEA. The arrows indicate the impedance calculated from the slope of the polarization curve shown in Fig. 1. Comparison between the impedance data for the aged sample and the dc limit of 2.37 Ω cm^2 suggests that a low-frequency inductive loop could have been obtained at frequencies much smaller than the 10 mHz lower limit used here.

A complementary piece of electrochemical information can be obtained by examination of the high-frequency part of the impedance measurement. The high-frequency part of the measurement was not purely capacitive, but instead showed features

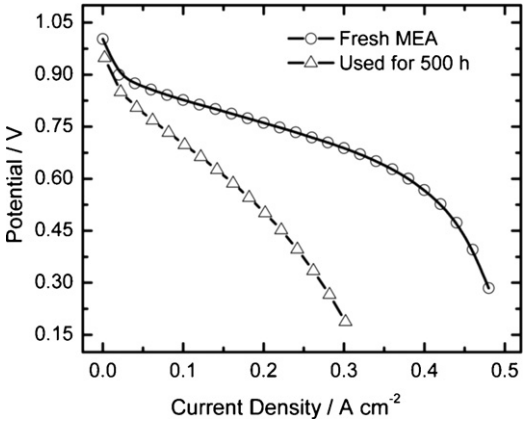

Fig. 1. The steady-state polarization curve with time of operation as a parameter. The anode reactant stream and cell temperatures were set at 40 °C and the cathode reactant stream temperature was set at 35 °C.

associated with constant-phase-element (CPE) behavior, i.e.,

$$Z(f) = R_e + \frac{1}{(j2\pi f)^{\alpha} Q_{eff}} \quad (2)$$

where R_e is the Ohmic resistance, f is the frequency, and $j = \sqrt{-1}$ is the imaginary number. The CPE parameters α and Q_{eff} are independent of frequency. The graphical methods presented by Orazem et al. [30] were used to obtain CPE parameters α and Q_{eff}. The parameter α was obtained from

$$\alpha = \left| \frac{d \log |Z_j|}{d \log f} \right| \quad (3)$$

where Z_j is the imaginary part of the impedance. The parameter Q_{eff} was obtained from

$$Q_{eff} = \sin\left(\frac{\alpha\pi}{2}\right) \frac{-1}{Z_j (2\pi f)^{\alpha}} \quad (4)$$

The parameters α and Q_{eff} obtained by graphical evaluation of Eqs. (3) and (4) are the same as would be obtained by regression analysis. Hirschorn et al. [31] have shown that the effective capacitance associated with a surface distribution of time constants in the presence of an Ohmic resistance can be expressed in terms of CPE parameters as

$$C_{eff} = Q_{eff}^{1/\alpha} R_e^{(1-\alpha)/\alpha} \quad (5)$$

which is equivalent to Eq. (5) presented by Brug et al. [32] for a blocking electrode. In a comparison of expressions developed by Hsu and Mansfeld [33] and Brug et al. [32], Huang et al. [34] found that Eq. (5) provided an excellent assessment of interfacial capacitance for systems for which the CPE behavior originated from

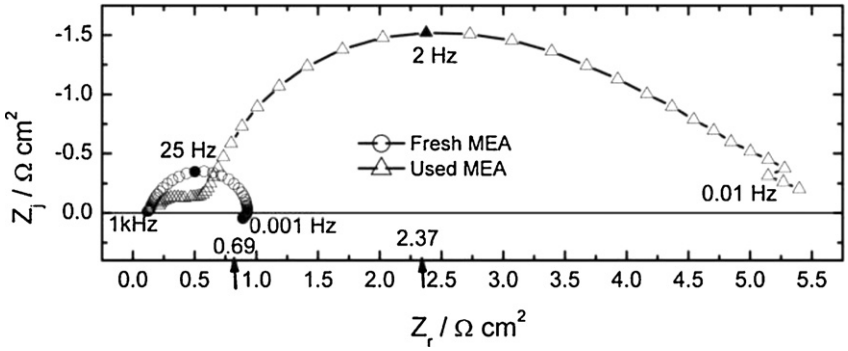

Fig. 2. Impedance responses collected at at 0.2 A cm^{-2} for the system described in Fig. 1 with time of operation as a parameter. The arrows indicate the impedance calculated from the slope of the polarization curve shown in Fig. 1.

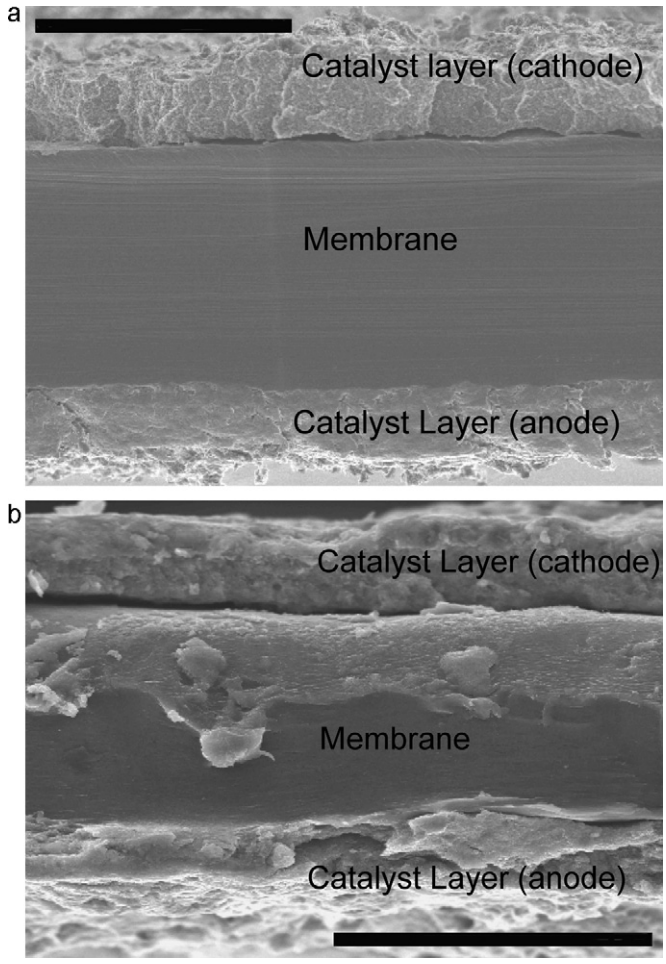

Fig. 3. SEM micrographs of MEA cross-sections taken at a 15 kV accelerating voltage. The bar length is 50 μm. The cross-sections of the both un-used and used MEA were cut with sharp razor and the samples were coated with Au–Pd: (a) un-used sample; and (b) aged sample.

nonuniform current and potential distributions along the electrode surface. Such 2D distributions may be expected for the fuel cell under study due to both the channel-land configuration and distributions of reactants and products along the length of the channels [35]. A further comparison of the different formulas for effective capacitance is provided by Hirschorn et al. [31].

The interfacial capacitance for the un-used sample was found to be 0.078 F cm^{-2}, and the corresponding value for the aged sample was 0.045 F cm^{-2}. These results suggest that the electrochemically active area of the aged MEA was only 58% of that of the new MEA. The decrease in the electrochemically active area may attributed to catalyst dissolution, agglomeration, and/or deactivation. The results obtained here are consistent with the decay of active surface area observed by Roy and Orazem [35,36] over a shorter period of time.

3.2. Surface analysis

The ex situ surface techniques used included scanning electron microscopy (SEM), transmission electron microscopy (TEM), X-ray photoelectron spectroscopy (XPS), and X-Ray Diffraction (XRD).

3.2.1. Scanning electron microscopy

Morphology changes of the electrode-membrane interface can be clearly seen in the SEM images of MEA cross sections presented in Fig. 3. Changes in surface features were observed between the un-used (Fig. 3(a)) and the used (Fig. 3(b)) catalyst layers. These types of changes have been described as mud-cracking and surface erosion and have been explained to be a result of the loss of catalyst particle or loss of recast Nafion® ionomer from the catalyst surface due to particle dissolution [18].

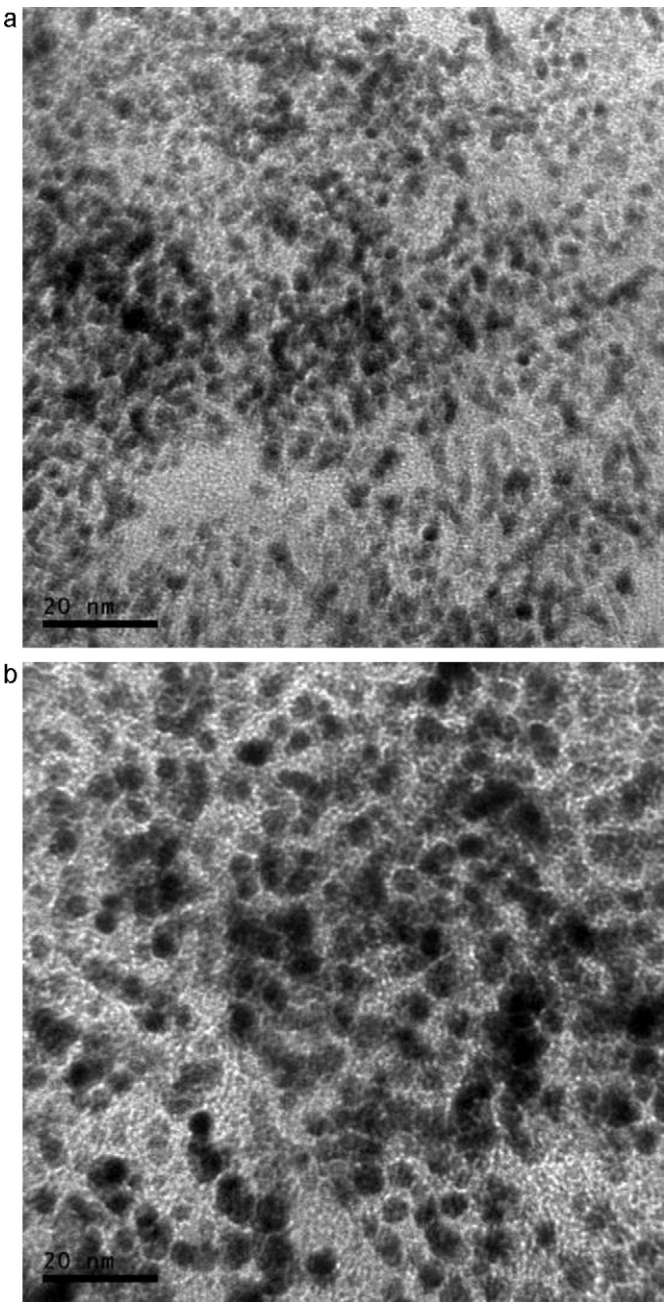

Fig. 4. TEM images obtained from the MEA cathode catalyst layers: (a) as received; and (b) after 600 h of operation. The bar length is 20 nm.

3.2.2. Transmission electron microscopy

Both un-used and used cathode catalyst layers were subjected to TEM measurements to explore changes with extended operation in the fuel cell. Representative high-resolution TEM pictures are presented in Fig. 4. As is evident in Fig. 4, the particle sizes in the catalyst layer are larger after 600 h of operation compared to the un-used particles.

The decrease in the electrochemically active surface area could be due to the combined influence of metal catalyst cluster agglom-

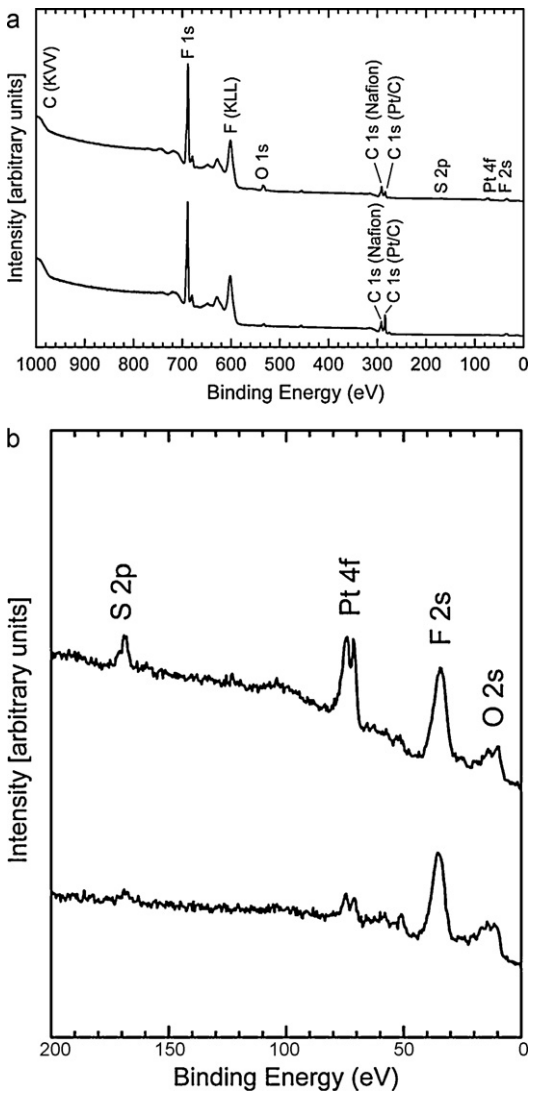

Fig. 5. XPS survey spectra obtained from MEA cathode catalyst layers. The lower line is as received, and the upper line is after 600 h of operation: (a) survey spectrum; and (b) zoom of the low-energy region.

eration or loss of support particles and metal clusters from the catalyst layer [18]. Due to weak bonding of platinum particles with the carbon support, the formation of catalyst particle agglomerates is possible. The decreased surface area has also been attributed to platinum dissolution and redeposition at the catalyst/ectrolyte interface [17]. The migration of the platinum particles to the membrane interface has also been reported [19]. Once catalyst particles have migrated into the membrane, they would lose electrical contact with the catalyst layer, which could also cause the loss of the electrochemical active surface area.

3.2.3. X-ray photoelectron spectroscopy

The XPS survey spectra obtained from the un-used and used MEA cathode catalyst layers are presented in Fig. 5(a). The lower line represents the results obtained for the un-used as received MEA, and the upper line represents the results obtained for the MEA after 600 h of operation. To show more clearly the peaks obtained for binding energies below 200 eV, a zoom of the low energy region is presented in Fig. 5(b). The main peaks in both spectra are due to fluorine and carbon. The fluorine and some of the carbon are due to the Nafion® content in the catalyst layer. Two distinct peaks of carbon are discerned in the survey spectra presented in Fig. 5(a),

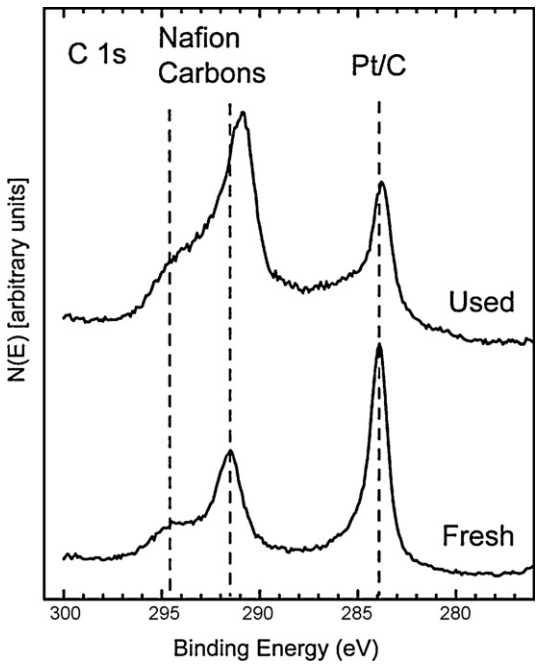

Fig. 6. C 1s high-resolution spectra obtained from un-used and used (after 600 h of operation) MEA cathode catalyst layers.

one due to the carbon from the Nafion® content in the catalyst layer and one due to adventitious carbon as well as the carbon support of the Pt/C catalyst.

Closer examination of the high-resolution spectra from the C 1s region, shown in Fig. 6, reveals two Nafion®-related carbon peaks between binding energies of 291 and 294 eV. On the un-used catalyst, the ratio of support carbon to Nafion® carbon is higher than on the used catalyst. It appears that, after extended operation in the fuel cell, either the Nafion® content is higher at the surface of the catalyst layer, or the support carbon content is significantly lower. This could be due to migration of Nafion® onto the catalyst layer from the Nafion® membrane due to membrane degradation, or to carbon support corrosion, or both. The shift in binding energies of the Nafion® carbon peaks (to lower binding energies) may indicate some degradation of the membrane, which would explain how membrane fragments migrate to the catalyst layer. The higher oxygen and sulfur concentrations on the used catalyst layer would also support this interpretation. However, considering the significantly higher Pt-to-C ratio after extended hours of operation, support corrosion may also take place. Carbon support degradation would lead to removal of carbon support and perhaps also to platinum migration, both of which could increase the Pt-to-C ratio at the outermost surface of the catalyst layer.

The high-resolution spectra of the Pt 4f region are presented in Fig. 7. The binding energies of the Pt 4f peaks (~71 eV) are consistent with those reported for Pt metal [37]. Since the spectra have been normalized, the lower Pt content on the un-used catalyst layer is evident in the lower signal-to-noise ratio of the spectrum obtained from this sample. In addition to a higher Pt content on the used cathode catalyst layer, the Pt 4f peaks are broader compared to the un-used cathode catalyst layer. There is a significant shoulder at higher binding energies compared to Pt metal. This is indicative of Pt oxidation. In fact, the Pt 4f spectrum obtained from 3 monolayers (ML) of PtO_x on Pt(1 0 0), prepared using atomic oxygen, is very similar to the spectrum obtained from the used catalyst layer [38]. This suggests that the amount of oxidized Pt in the near surface region of the catalyst is similar to the amount of oxidized Pt in a 3 ML PtO_x film on a single crystal Pt surface. However, the XPS data

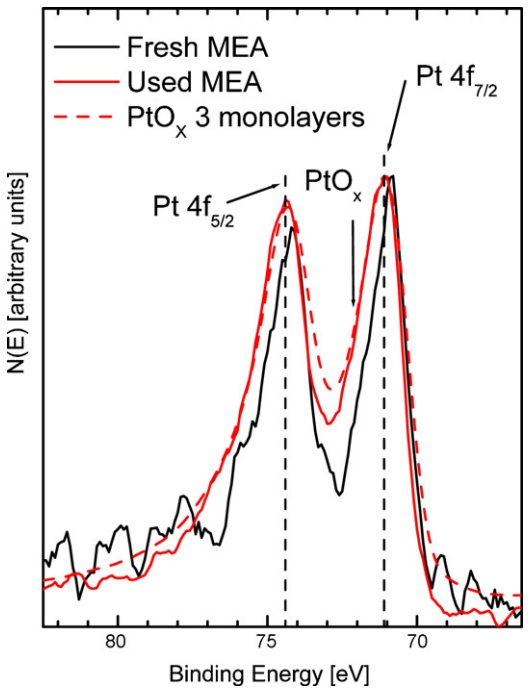

Fig. 7. Pt 4f high-resolution spectra obtained from un-used and used (after 600 h of operation) MEA cathode catalyst layers.

does not reveal how the oxidized Pt is distributed on the surface, i.e., whether small particles contain more Pt at a higher oxidation state, or if the amount of surface Pt oxidation is relatively uniform. Also, while there is unmistakable evidence that some of the original Pt metal on the surface of the catalyst is at a higher oxidation state, it is not possible to determine from the Pt 4f peaks whether the shoulder is due to PtO_x or $Pt(OH)_y$.

The XPS data reveal that, after extended operation in the fuel cell, some of the platinum in the catalyst layer has been oxidized. It is worth noting that the Pt 4f shoulder from the 3 ML oxide is small because the electron kinetic energy for that peak is large (~1180 eV), which means a lower surface sensitivity compared with electrons at higher binding energies. The higher O 1s intensity in the spectrum obtained from the used catalyst layer is in agreement with the formation of PtO_x or $Pt(OH)_y$ and a higher content of sulfates as compared to the un-used catalyst layer.

3.2.4. X-ray diffraction

The XRD spectra obtained from the un-used and used MEA catalyst layers are presented in Fig. 8. Peaks due to crystalline Pt metal are evident in both spectra. The main difference between the un-used and the used data is that higher intensity Pt peaks were obtained from the used catalyst layer. This suggests that the particle sizes of the crystalline Pt are larger on the used catalyst layer as compared to the un-used catalyst layer. The average Pt particle sizes, calculated using the full width at half maximum (FWHM) of the Pt(1 0 0) peak at $2\theta = 39.9^\circ$ and the Scherrer equation, are ~2.7 nm on the un-used catalyst layer and ~3.4 nm on the used catalyst layer. The increased Pt particle size on the used catalyst layer, apparent from the XRD data, was also observed in the TEM images shown in Fig. 4. These results suggest that Pt has some mobility on the support.

3.3. Effluent analysis

A trace amount of platinum, 0.6 ppb, was found in the cathode effluent by ICP-MS, which could be attributed to loss of catalyst

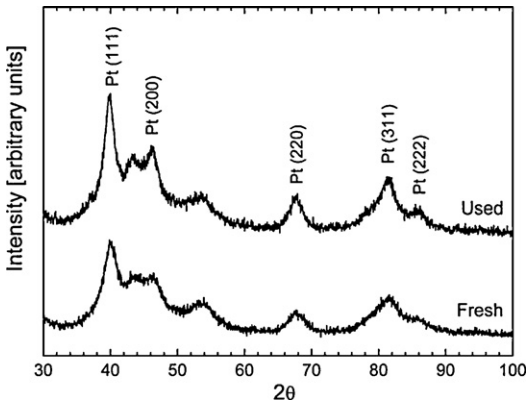

Fig. 8. XRD spectra obtained from un-used and used (after 600 h of operation) MEA cathode catalyst layers.

[18]. The presence of the quantifiable amount of the platinum in the outlet water has also been explained as being a result of platinum dissolution [17]. Platinum dissolution was included in the reaction scheme proposed by Darling and Meyers [13] and incorporated into the impedance model developed by Roy et al. [9].

4. Discussion

Recent work in the literature, notably that of Zhang et al. [23,26], Rinaldo et al. [24], and Liu et al. [25], has established that formation and dissolution of platinum oxides or hydroxides can serve as a mechanism for degradation of PEM fuel cell performance. The impedance model developed by Roy et al. [9] showed that low-frequency inductive loops could potentially be attributed to a reduction in catalytic activity associated with platinum oxidation. The present work demonstrates by XPS that oxidized platinum was formed during operation of the PEM fuel cell studied by Roy et al. [9]. The used MEA was characterized by a cell impedance that was 5 times larger than its initial value, and the high frequency part of the impedance showed a reduction of active area in the used cell to 58% of its initial value. The low-frequency part of the impedance showed, initially, a clearly define inductive loop that was obscured after 600 h of use. The present work supports the argument that the low-frequency inductive loop is associated with platinum oxidation.

The Darling–Meyer model assumes that the PtO_x is formed and then dissolves. The results of ICP-MS experiments indicated that the dissolution reaction, if present, takes place at a very slow rate. The attribution of the low-frequency inductive loop to platinum oxidation, however, is not sensitive to the rate of platinum dissolution. This explanation, however, is sensitive to the reversibility of platinum oxidation as a function of potential. While the reversibility of platinum oxidation was not addressed in the present work, it was addressed by Liu et al. [25] who report that the reaction is indeed reversible.

The present work can be used as an example of the need to couple impedance measurements with other observations. Orazem and Tribollet [27] articulated a philosophy for interpretation of impedance measurements that integrates experimental observation, model development, and error analysis. It takes into account the fact that impedance spectroscopy is not a stand-alone technique and that other observations are required to validate a given interpretation of the impedance spectra. Within the context of the work presented here, the objective of modeling is not to provide a good fit with the smallest number of parameters, but, rather, to use the model to learn about the physics and chemistry of the system under study.

5. Conclusions

The interpretation of the low-frequency inductive loops observed by Roy and Orazem [4] in terms of platinum oxidation was supported by the ex situ surface analysis. An amount of oxidized platinum equivalent to 3 ML of PtO_x was observed by XPS after 600 h of use in the fuel cell. The XRD and TEM data indicated that Pt agglomeration was also taking place. These results are consistent with the reduction in electrochemically active area inferred from the evaluation of interfacial capacitance. The ICP-MS data were less definitive, but suggested that trace amounts of Pt could be found in the fuel cell effluent. This result further supports the reaction sequence suggested by Darling and Meyers [13] and incorporated into the impedance model developed by Roy et al. [9].

Taken as a whole, these results support the premise that the low-frequency inductive features seen in the impedance response provide information useful for understanding phenomena, such as platinum oxidation, that lead to reduction of fuel cell performance. The capacitance data, taken from the high-frequency portion of the impedance spectrum, yield information on the reduction of electrochemically active area.

Acknowledgements

This work was supported by the NASA Glenn Research Center under grant NAG 3-2930 monitored by Timothy Smith with additional support from Gamry Instruments Inc. The SEM, TEM, XPS, and XRD measurements were performed at the University of Florida Major Analytical and Instrumentation Center (MAIC), and the ICP-MS measurements were performed in the Department of Chemistry at the University of Florida. The staff at MAIC is gratefully acknowledged for their technical support and professional advice. Luke Neal performed the XRD and particle sizing analysis, and Professor Jason Weaver (University of Florida) provided the reference PtO_x XPS spectrum with 3 monolayers of oxide. Their assistance is gratefully acknowledged.

References

[1] R. Makharia, M.F. Mathias, D.R. Baker, J. Electrochem. Soc. 152 (2005) A970–A977.
[2] O. Antoine, Y. Bultel, R. Durand, J. Electroanal. Chem. 499 (2001) 85–94.
[3] Y. Bultel, L. Genies, O. Antoine, P. Ozil, R. Durand, J. Electroanal. Chem. 527 (2002) 143–155.
[4] S.K. Roy, M.E. Orazem, J. Electrochem. Soc. 154 (2007) B883–B891.
[5] P. Agarwal, M.E. Orazem, L.H. García-Rubio, J. Electrochem. Soc. 139 (1992) 1917–1927.
[6] P. Agarwal, O.D. Crisalle, M.E. Orazem, L.H. García-Rubio, J. Electrochem. Soc. 142 (1995) 4149–4158.
[7] P. Agarwal, M.E. Orazem, L.H. García-Rubio, J. Electrochem. Soc. 142 (1995) 4156–4159.
[8] M.E. Orazem, J. Electroanal. Chem. 572 (2004) 317–327.
[9] S.K. Roy, M.E. Orazem, B. Tribollet, J. Electrochem. Soc. 154 (2007) B1378–B1388.
[10] C.F. Zinola, J. Rodriguez, G. Obal, J. Appl. Electrochem. 31 (2001) 1293–1300.
[11] A. Damjanovic, V. Brusic, Electrochim. Acta 12 (1967) 615–628.
[12] V.O. Mittal, H.R. Kunz, J.M. Fenton, Electrochem. Solid-State Lett. 9 (2006) A229–A302.
[13] R.M. Darling, J.P. Meyers, J. Electrochem. Soc. 150 (2003) A1523–A1527.
[14] T. Patterson, Fuel Cell Technology Topical Conference Proceedings. AIChE Spring National Meeting, 2002, p. 235.
[15] M. Mathias, D. Baker, J. Zhang, Y. Liu, W. Gu, ECS Trans. 13 (13) (2008) 129–152.
[16] C. Roth, M. Goetz, H. Fuess, J. Appl. Electrochem. 31 (2001) 793–798.
[17] J. Xie, D.L. Wood, K.L. More, P. Atanassov, R.L. Borup III, J. Electrochem. Soc. 152 (2005) A1011–A1020.
[18] J. Xie, D.L. Wood, D.M. Wayne, T.A. Zawodzinski, P. Atanassov, R.L. Borup III, J. Electrochem. Soc. 152 (2005) A104–A113.
[19] P.J. Ferreira, G.J. la O', Y. Shao-Horn, D. Morgan, R. Makharia, S. Kocha, H.A. Gasteiger, J. Electrochem. Soc. 152 (2005) A2256–A2271.
[20] M. Chatenet, E. Guilminot, C. Iojoiu, J.Y. Sanchez, E. Rossinot, F. Maillard, ECS Trans. 11 (1) (2007) 1203–1214.
[21] F.Y. Zhang, S.G. Advani, A.K. Prasad, M.E. Boggs, S.P. Sullivan, T.P. Beebe Jr., Electrochim. Acta 54 (2009) 4025–4030.
[22] S. Zhang, X.Z. Yuan, J.N.C. Hin, H. Wang, K.A. Friedrich, M. Schulze, J. Power Sources 194 (2009) 588–600.
[23] F.Y. Zhang, S.G. Advani, A.K. Prasad, M.E. Boggs, S.P. Sullivan, P. Thomas, J. Beebe, Electrochim. Acta 54 (2009) 4025–4030.
[24] S.G. Rinaldo, J. Stumper, M. Eikerling, J. Phys. Chem. C 114 (2010) 5773–5785.
[25] Y. Liu, M. Mathias, J. Zhang, Electrochem. Solid-State Lett. 13 (2010) B1–B3.
[26] S. Zhang, X.Z. Yuan, J.N.C. Hin, H. Wang, J. Wu, K.A. Friedrich, M. Schulzeb, J. Power Sources 195 (2010) 1142–1148.
[27] M.E. Orazem, B. Tribollet, Electrochim. Acta 53 (2008) 7360–7366.
[28] B. Hirschorn, B. Tribollet, M.E. Orazem, Isr. J. Chem. 48 (2008) 133–142.
[29] D.A. Blom, J.R. Dunlap, T.A. Nolan, L.F. Allarda, J. Electrochem. Soc. 150 (2003) A414–A418.
[30] M.E. Orazem, N. Pébère, B. Tribollet, J. Electrochem. Soc. 153 (2006) B129–B136.
[31] B. Hirschorn, M.E. Orazem, B. Tribollet, V. Vivier, I. Frateur, M. Musiani, Electrochim. Acta 55 (2010) 6218–6227.
[32] G.J. Brug, A.L.G. van den Eeden, M. Sluyters-Rehbach, J.H. Sluyters, J. Electroanal. Chem. 176 (1984) 275–295.
[33] C.H. Hsu, F. Mansfeld, Corrosion 57 (2001) 747–748.
[34] V.M.W. Huang, V. Vivier, M.E. Orazem, N. Pébère, B. Tribollet, J. Electrochem. Soc. 154 (2007) C99–C107.
[35] S.K. Roy, M.E. Orazem, J. Electrochem. Soc. 156 (2009) B203–B209.
[36] S.K. Roy, M.E. Orazem, J. Power Sources 184 (2008) 212–219.
[37] J. Moulder, W. Stickel, P. Sobol, K. Bomben, Handbook of X-Ray Photoelectron Spectroscopy, Physical-Electronics, Inc., Eden Prairie, MN, 1995.
[38] R.B. Shumbera, H.H. Kan, J.F. Weaver, Surf. Sci. 601 (2007) 235–246.